THE ASTROPHYSICAL JOURNAL, 179:731–754, 1973 February 1

VARIATIONS IN SPECTRAL-ENERGY DISTRIBUTIONS AND ABSORPTION-LINE STRENGTHS AMONG ELLIPTICAL GALAXIES

S. M. FABER*
Harvard University
Received 1972 August 3

ABSTRACT

Thirty-one elliptical galaxies and 10 globular clusters have been observed on a 10-color intermediate-band photometric system designed for the study of old stellar populations. To within the accuracy of the present data, the integrated colors of elliptical galaxies can be specified with only two independent parameters which in turn may be utilized to determine both the intrinsic colors and the reddening between the galaxy and the observer. The intrinsic colors and line strengths are closely correlated with absolute magnitude at all luminosities.

Most of the galaxies observed are members of pairs or small groups. No variations in galaxy colors were found that correlated with group properties, morphological types of companions, or the presence of optical line or radio emission. In short, these integrated colors of elliptical galaxies are independent of all physical properties studied other than luminosity.

The strengths of the absorption features CN and Mg "b" plus MgH, together with blanketing by metallic lines near 3800 Å, increase monotonically with increasing luminosity. A reddening-free line absorption index monitoring CN and Mg can be used to determine the absolute magnitude of an elliptical galaxy with an accuracy of ± 0.56 mag.

Estimates of the integrated color and absorption-line changes expected solely from variations in metal abundance have been calculated for an old stellar population with a main-sequence turnoff near 1 $\mathfrak{M}_\odot$. The difference in color and line strength between M32 and the most luminous elliptical galaxies is consistent with an increase in [Fe/H] from the solar value in M32 to twice the solar value in luminous ellipticals. The uncertainties in this result are discussed.

Subject headings: galaxies, photometry of — globular clusters

I. INTRODUCTION

Most photometric studies of elliptical galaxies have emphasized that these objects form a fairly homogeneous family. Integrated color indices of ellipticals generally fall within restricted limits, and many investigators (Baum 1959; de Vaucouleurs 1961; Hodge 1963; Webb 1964; Rood 1969; Tifft 1969; Lasker 1970; and others) have noted that intrinsically faint ellipticals tend to be bluer than more luminous ones. The reddening-free metallicity index Q also increases monotonically with luminosity (McClure and van den Bergh 1968*a*). These results imply that the stellar population of an elliptical galaxy is closely related to its absolute magnitude.

However, careful inspection of these data reveals a considerable amount of scatter larger than the quoted observational errors within the color-color and color-magnitude diagrams published to date. Significant differences also exist among the mean relations between color and absolute magnitude determined by various investigators. (See Faber 1971 for a more complete discussion of these results.) Several factors might introduce spurious differences among the color-magnitude diagrams in various studies. Not all investigators present colors corresponding to a standard diameter defined in the

* National Science Foundation Predoctoral Fellow, Carnegie Institution of Washington Predoctoral Fellow, and Visiting Student, Kitt Peak National Observatory, which is operated by the Association of Universities for Research in Astronomy, Inc., under contract with the National Science Foundation. Present address: Lick Observatory, Board of Studies in Astronomy and Astrophysics, University of California, Santa Cruz.

same way for all galaxies independent of size or absolute magnitude. Color-magnitude relations might be different in various color systems. Inaccurate corrections for reddening in our own Galaxy will introduce additional errors.

On the other hand, evidence of a somewhat different nature suggests that at least some of this scatter is real and that the stellar content of elliptical galaxies cannot be completely specified with just one parameter, the luminosity. From photographic photometry of double nebulae, Holmberg (1958) concluded that the stellar populations and surface brightnesses of both galaxies in a pair were similar. This result applied to ellipticals indicates that the mean colors and stellar populations of E galaxies in pairs should correlate with the morphological type of the companion galaxy. Unfortunately Holmberg's data on ellipticals were too scanty to verify this prediction. Hodge (1963) found that the *UBV* colors of elliptical nebulae in two close, interacting pairs were abnormal, while Fish (1964) suggested that the mass-to-light ($\mathfrak{M}/L$) ratios of E galaxies with late-type galaxy companions were systematically lower than $\mathfrak{M}/L$ ratios for those with early-type companions. This result supported Holmberg's contention that the properties of pair members are correlated. Lastly, a small number of peculiar dwarf ellipticals are known that are quite red and have unusually high surface brightness. These strange objects clearly do not fit into the sequence of normal ellipticals.

In the present study, integrated photometry in 10 colors on 33 galaxies has been used to test whether elliptical galaxies actually form a one-parameter sequence. The elliptical galaxies observed span a range in luminosity of almost 6 mag. Nearly all are members of pairs or small groups. In some cases these groups are subsets of larger clusters, while in others the group is an isolated unit. Eleven galaxies are listed in Arp's (1966) *Atlas of Peculiar Galaxies*, six of which interact visibly with their companions. Types of companions range from E to Irr I. At least five of the objects are radio sources. In short, these elliptical galaxies exhibit a wide variety of physical properties. In the present paper, we show that in fact only one of these properties, the luminosity, is significantly correlated with the integrated photometric indices.

II. SELECTION OF PAIRS

Holmberg (1937) has described a criterion for selecting physically associated double galaxies from a population of galaxies randomly arranged on the sky. This criterion was adopted as a starting point in choosing candidates for observation in this study. Let D_1 and D_2 represent the diameters of two pair members and S the separation between them. Holmberg has shown that if the apparent photographic magnitudes of both galaxies are less than 15.7 mag and $S \leq 2(D_1 + D_2)$, then the probability that the pair is an optical double—that is, physically unrelated—is only 13 percent. The contrast between optical and physical doubles can be increased by applying Holmberg's criterion to a set of galaxies with brighter limiting magnitude. In general, the limiting photographic magnitude of pair members in this study was 14.0. For this case, less than 6 percent of the pairs chosen according to Holmberg's criterion are optical pairs. Since Holmberg's analysis assumes that the galaxies are randomly arranged on the sky, his criterion has no validity in large clusters, where the probability of chance alignment is higher. Some of the objects considered here are members of large clusters, and, except as noted, no claim is made for pair membership in these cases.

When the radial velocities available for both members of a possible pair were similar, in a few cases Holmberg's criterion was relaxed by a factor of 2. Page's (1961) list of double galaxies with measured velocities indicates that true physical doubles sometimes have radial velocities that differ by as much as 650 km s^{-1}. Accordingly, if two galaxies with $\Delta v \leq 650$ km s^{-1} also had a separation $S \leq 4(D_1 + D_2)$, they were accepted as candidates for observation. With one exception, at least one radial velocity was required for each pair or group, since too large a velocity would shift important spectral features out of the filter bandpasses. This upper limit was set at

4000 km s^{-1}. The great majority of pairs finally chosen satisfied both the more stringent version of Holmberg's criterion and the velocity criterion and so are of high reliability.

Table 1 identifies the galaxies observed, together with information concerning their pair or group membership. Column (1) contains the NGC number of the object or its designation in the *Reference Catalogue of Bright Galaxies* (RCBG) (de Vaucouleurs and de Vaucouleurs 1964). Column (2) lists all the members in the immediate group of which the object is a member, determined according to the criteria already set forth. Column (3) indicates membership in a larger aggregate, if any. Morphological types according to de Vaucouleurs from the RCBG are found in column (4).

III. PHOTOMETRIC SYSTEM AND OBSERVATIONS

Previous investigators have used two intermediate-band photometric systems for the study of old stellar populations, the 5-color David Dunlap Observatory (DDO)

TABLE 1

E GALAXIES WITH 10-COLOR PHOTOMETRY

Name (1)	Immediate Group Members (2)	Larger Aggregate (3)	Galaxy Type (4)
NGC 205	205, 221, 224	Local Group	E+5p
221	205, 221, 224	Local Group	E2
584	584, 586, 596		E4
596	584, 586, 596		E0
1332	1331, 1332, I324	1315-1332 Group*	S0:
1889	1888, 1889		E0
2300	2276, 2300		E+2
2634	2634, 2634A	Probably in a group	E1:
2672	2672, 2673	Probably in a group*	E1-2
2872	2872, 2874		E?
3073	3073, 3079		Ep?
3193	3185, 3187, 3190, 3193	3193 Group*†	E2
3226	3226, 3227		E+2p:
3379	3377, 3379, 3384	Leo Group*†	E+1
3605	3605, 3607, 3608	3607 Group*	E4-5
3608	3605, 3607, 3608	3607 Group*	E2
3613	3613, 3619	3642 Group†	E+6
4261	4260, 4261, 4264	Group W-a ‡	E2-3
4278	4274, 4278, 4283	4274 Group†	E1-2
4283	4274, 4278, 4283	4274 Group†	E0
4464		Virgo Cluster	E2
4472		Virgo Cluster	E2
4478		Virgo Cluster	E2
4486		Virgo Cluster	E0-1p
4486B		Virgo Cluster	E0
4627	4627, 4631, 4656-7	Canes Venatici Cluster§	E+p
4649	4647, 4649	Virgo Cluster	E2
5846	5846, 5846A, 5850	5846 Group	E+0-1
5846A	5846, 5846A, 5850	5846 Group	E2-3
5982	5981, 5982, 5985		E3
6307	6306, 6307		E4:
7619		Peg I Cluster	E3
7626		Peg I Cluster	E1

*Vaucouleurs and Vaucouleurs, Reference Catalogue of Bright Galaxies, notes, 1964.

†Van den Bergh, Ap.J., 131, 215, 1960.

‡Vaucouleurs, Ap.J. Supp., 5, 233, 1961.

§Van den Bergh, Ap.J., 131, 558, 1960.

system (McClure and van den Bergh 1968*b*) and Wood's (1966, 1969) 12-color system. Examination of published scans of elliptical galaxies (Oke and Sandage 1968; Schild and Oke 1971; Whitford 1971) indicates that the DDO and Wood systems taken together monitor the most significant absorption features in elliptical-galaxy spectra. Therefore, a combination of these two systems offers a reasonably complete intermediate-bandpass filter set for elliptical galaxies and at the same time affords access to a considerable body of data already published. In order to maximize efficiency, certain of Wood's filters were omitted. The characteristics of the 10 filters ultimately adopted are presented in table 2.

Because of the Doppler effect, relative motion between the source and observer produces a change in the effective wavelength of the observing passbands as measured in the rest frame of the object. As a result, redshifts greater than 2000 km s^{-1} will have a nonnegligible effect on colors of elliptical galaxies measured with six of the filters used in the present study. Therefore, galaxies with redshifts greater than 1500 km s^{-1} were observed with an alternate set of six filters having passbands shifted to longer wavelengths. The amount of this shift corresponded to a recessional velocity of approximately 1500 km s^{-1} relative to the rest wavelengths of the original system. Table 2 indicates which bandpasses possessed filters at both rest and redshifted wavelengths. (In table 2, Δv is the differential velocity in km s^{-1} between the zero-velocity and redshifted members of the pair.) The methods used to further correct the observations for the effect of redshift are described below.

Most of the observations were taken at the Cassegrain focus of the Number 2 36-inch (91-cm) reflector of the Kitt Peak National Observatory. The signal from an ITT FW-130 photomultiplier was measured in the pulse-counting mode with a fast amplifier-discriminator and a digital counter. All observations of NGC 4464, 4627, 5982, 6307, and partial observations of certain other galaxies were obtained with the 61-inch (155-cm) Mount Hopkins reflector of the Smithsonian Astrophysical Observatory.

On a 36-inch telescope, measurements of fairly faint objects through relatively narrow filters are limited by the sky background. With apertures comparable to D_0, the diameter of the galaxy given in the RCBG, the sky counts in the four bluest filters overwhelm the galaxy signal. Consequently, smaller aperture sizes were chosen that

TABLE 2

PHOTOMETRIC SYSTEM IN THIS PAPER

Filter	Source	λ_{eff} (Å)	Half-width (Å)	Δv (km s^{-1})	Spectral Feature Monitored
35.....	DDO, Wood	3450	390		Balmer discontinuity
38.....	DDO	3803 3818	140	1180	Line-blanketing discontinuity
41.....	DDO	4167 4181	79	1070	CN absorption
42.....	DDO	4257 4275	82	1270	G-band
45.....	DDO	4517 4543	84	1730	
52.....	Wood	5162 5195	54	1910	MgH + Mg "b"
55.....	Wood	5545	214		Continuum
62.....	Wood	6222 6257	108	1690	TiO
67.....	Wood	6702	131		Continuum
74.....	Wood	7415	188		Continuum

approximate the diameter of the object on the E plate of the *Palomar Sky Survey* when that diameter is less than or equal to 65 arc seconds, the largest diaphragm size available. A discussion of aperture effects below shows that this procedure has not introduced significant errors. Diaphragm sizes, A, in seconds of arc, together with A/D_0, are given for all objects in table 3.

The magnitudes in this paper have been reduced to an absolute energy system through observations of standard stars published by Oke (1964) and Hayes (1970) and corrected to the revised calibration of α Lyr determined by Oke and Schild (1970). A magnitude on this system represents the mean incident energy in magnitudes per unit frequency over the passband of the filter, weighted by the total response function of the observing system. The methods employed in reducing the magnitudes to an absolute energy system are described more fully by Faber (1971). Colors on this system are formed relative to filter 55.

Table 3 presents the average colors measured for all galaxies and globular clusters, together with the internal mean error in magnitudes associated with each color. "Filter set" refers to the zero-point velocity in km s^{-1} of the filter set used for the observation.

IV. CORRECTIONS TO OBSERVED COLORS

The colors in table 3 must be corrected for the effects of redshift and galactic reddening. Redshift corrections to colors (as distinct from magnitudes) entail only a correction for the shift of a different region of the spectrum into the passband of the system. For filter 55, effects of redshift up to 4000 km s^{-1} are negligible. For filters 67 and 74, the corrections depend on the fine structure in the spectra and hence are quite uncertain. In any case, the corrections are less than 0.01 mag for most galaxies and were ignored. For filter 35, corrections are impossible to compute since the published scans of nearby galaxies beyond 3375 Å do not extend to sufficiently short wavelengths. However, Oke's (1971) photometry of distant ellipticals with significant redshifts indicates that the slope of the continuum does not increase significantly shortward of 3375 Å. With this assumption, the correction is less than 0.04 mag at a velocity of 4000 km s^{-1}. Because this effect is small and because all but six of the galaxies observed have redshifts of less than 2500 km s^{-1}, no corrections were applied to the (35 − 55) index.

The effects of redshift on the remaining six colors, each of which can be measured through either an unredshifted or redshifted filter, were estimated in two ways. Oke standard stars were used to calibrate both the shifted and unshifted sets of filters. Hence, magnitudes on both sets are measures of the mean energy per unit frequency in the galaxy continuum at both the zero-velocity and the redshifted wavelengths. Four galaxies with velocities near 1500 km s^{-1} (NGC 584, 4486, 4649, and 5846) were measured through both sets of filters, and the colors were compared. The differences (table 4) describe the errors incurred by measuring a galaxy with a redshift v_g that is 1500 km s^{-1} larger than the velocity of the filter set, v_f. Table 4 also includes the expected errors, estimated from published galaxy scans. The errors found in the two different ways agree closely. The observed errors were used to correct the galaxy colors in table 3 under the assumption that the correction required is a linear function of $(v_g - v_f)$.

A cosecant law for galactic reddening was used to approximately correct the galaxy colors for the effect of reddening in the Milky Way. The correction for each color index was of the form $K_{(x-55)} \csc b$, where b is the galactic latitude of the object. A coefficient of 0.05 mag in $E(B - V)$ for reddening at the galactic pole was adopted, as suggested by de Vaucouleurs and Malik (1969) for use with bright galaxies. The correction for each of the 10 passbands was derived from Whitford's (1958) reddening

TABLE 3

ORIGINAL COLORS OF ELLIPTICAL GALAXIES AND GLOBULAR CLUSTERS

Name	Aperture (arc sec)	Number of observations	Filter set	(35-55) (mag)	(38-55) (mag)	(41-55) (mag)	(42-55) (mag)	(45-55) (mag)	(52-55) (mag)	(62-55) (mag)	(67-55) (mag)	(74-55) (mag)
NGC 584	39.3*	4	1500	+2.391	+2.099	+1.206	+1.076	+0.608	+0.349	-0.228	-0.401	-0.648
				0.014	0.010	0.014	0.018	0.009	0.012	0.005	0.003	0.009
596	55.0	4	1500	+2.291	+1.963	+1.104	+1.027	+0.586	+0.308	-0.203	-0.384	-0.603
				0.034	0.021	0.022	0.014	0.006	0.009	0.020	0.010	0.014
1332	47.1	6	0	+2.560	+2.229	+1.324	+1.198	+0.675	+0.351	-0.233	-0.428	-0.680
				0.008	0.006	0.002	0.010	0.006	0.009	0.008	0.006	0.008
1889	15.5	6	1500	+2.328	+1.911	+1.150	+1.028	+0.604	+0.278	-0.275	-0.421	-0.647
				0.017	0.020	0.024	0.020	0.024	0.009	0.018	0.015	0.018
2300	55.0	5	1500	+2.675	+2.318	+1.411	+1.233	+0.710	+0.391	-0.280	-0.474	-0.773
				0.008	0.017	0.016	0.008	0.015	0.012	0.013	0.009	0.010
2634	31.4	5	1500	+2.335	+2.034	+1.172	+1.064	+0.589	+0.323	-0.186	-0.399	-0.625
				0.018	0.019	0.005	0.013	0.009	0.010	0.013	0.008	0.005
2672	39.3	5	1500	+2.526	+2.112	+1.225	+1.150	+0.672	+0.309	-0.266	-0.432	-0.654
				0.015	0.022	0.013	0.012	0.014	0.005	0.012	0.012	0.009
2872	31.4	3	1500	+2.498	+2.202	+1.271	+1.161	+0.637	+0.339	-0.221	-0.417	-0.665
				0.012	0.025	0.048	0.035	0.017	0.018	0.023	0.015	0.021
3073	19.9	5	0	+1.657	+1.220	+0.552	+0.472	+0.305	+0.119	-0.181	-0.322	-0.428
				0.021	0.034	0.024	0.026	0.014	0.014	0.020	0.015	0.027
3193	55.0	4	1500	+2.319	+2.028	+1.159	+1.061	+0.587	+0.331	-0.277	-0.391	-0.641
				0.016	0.003	0.008	0.010	0.007	0.008	0.011	0.004	0.006
3226	55.0	4	1500	+2.333	+1.920	+1.154	+1.037	+0.605	+0.311	-0.234	-0.424	-0.674
				0.022	0.010	0.018	0.009	0.010	0.014	0.015	0.015	0.019
3379	62.4	4	0	+2.429	+2.140	+1.233	+1.118	+0.619	+0.329	-0.249	-0.410	-0.681
				0.012	0.014	0.014	0.013	0.009	0.017	0.020	0.008	0.013
3605	46.2	6	0	+2.177	+1.856	+1.024	+0.977	+0.518	+0.249	-0.215	-0.358	-0.587
				0.030	0.036	0.009	0.021	0.023	0.022	0.014	0.024	0.041
3608	62.9	4	0	+2.342	+2.030	+1.141	+1.071	+0.608	+0.290	-0.230	-0.393	-0.642
				0.010	0.012	0.006	0.008	0.011	0.010	0.012	0.008	0.017
3613	54.6	5	1500	+2.337	+2.038	+1.143	+1.040	+0.558	+0.307	-0.225	-0.394	-0.612
				0.006	0.010	0.006	0.014	0.010	0.010	0.006	0.009	0.012
4261	66.6	4	1500	+2.460	+2.205	+1.277	+1.132	+0.609	+0.359	-0.216	-0.406	-0.657
				0.007	0.010	0.010	0.004	0.013	0.005	0.006	0.010	0.015
4278	62.4	4	0	+2.411	+2.039	+1.212	+1.126	+0.624	+0.346	-0.239	-0.430	-0.702
				0.014	0.009	0.010	0.012	0.011	0.006	0.005	0.006	0.003
4283	39.9	7	0	+2.337	+2.016	+1.156	+1.087	+0.610	+0.282	-0.195	-0.402	-0.655
				0.020	0.018	0.011	0.009	0.020	0.012	0.016	0.008	0.016
4464	27.0	7	0	+2.295	+2.013	+1.158	+1.085	+0.618	+0.295	-0.189	-0.371	-0.612
				0.009	0.016	0.004	0.006	0.006	0.004	0.003	0.005	0.011
4472	65.3	4	0	+2.524	+2.213	+1.290	+1.167	+0.633	+0.360	-0.228	-0.416	-0.687
				0.013	0.007	0.008	0.001	0.002	0.006	0.011	0.015	0.017
4478	15.2*	3	1500	+2.339	+2.031	+1.144	+1.063	+0.589	+0.344	-0.207	-0.391	-0.630
				0.012	0.005	0.025	0.005	0.021	0.016	0.026	0.008	0.003
4486	65.6	3	1500	+2.487	+2.208	+1.304	+1.141	+0.615	+0.405	-0.212	-0.427	-0.692
				0.021	0.007	0.016	0.004	0.010	0.013	0.007	0.002	0.005
4486B	13.7	5	0	+2.502	+2.197	+1.265	+1.140	+0.625	+0.358	-0.218	-0.404	-0.648
				0.021	0.026	0.017	0.016	0.017	0.006	0.012	0.001	0.021
4627	54.6	6	1500	+1.687	+1.142	+0.516	+0.495	+0.307	+0.143			
				0.016	0.007	0.027	0.018	0.018	0.010			
4649	61.7	3	1500	+2.559	+2.275	+1.320	+1.149	+0.613	+0.378	-0.246	-0.436	-0.706
				0.008	0.026	0.015	0.010	0.013	0.009	0.014	0.013	0.003
5846	55.0	3	1500	+2.616	+2.306	+1.334	+1.184	+0.663	+0.406	-0.232	-0.436	-0.712
				0.011	0.014	0.009	0.006	0.001	0.005	0.007	0.008	0.005
5846A	15.2	4	1500	+2.484	+2.129	+1.236	+1.141	+0.638	+0.356	-0.244	-0.431	-0.676
				0.022	0.023	0.021	0.023	0.016	0.018	0.010	0.009	0.011
5982	58.0	12	1500	+2.339	+2.033	+1.165	+1.045	+0.585	+0.293			
				0.007	0.010	0.005	0.004	0.006	0.014			
6307	39.4	4	1500	+2.313	+1.993	+1.135	+1.056	+0.611	+0.268	-0.240	-0.400	-0.596
				0.007	0.030	0.006	0.019	0.024	0.016	0.017	0.013	0.011
7619	55.0	4	1500	+2.627	+2.231	+1.344	+1.230	+0.676	+0.333	-0.306	-0.470	-0.700
				0.025	0.011	0.016	0.021	0.013	0.005	0.024	0.007	0.005
7626	55.0	3	1500	+2.611	+2.162	+1.283	+1.177	+0.656	+0.319	-0.274	-0.469	-0.701
				0.032	0.054	0.010	0.021	0.013	0.017	0.019	0.017	0.004
5024	63.0	2	0	+1.626	+1.166	+0.653	+0.619	+0.415	+0.135	-0.181	-0.285	-0.411
				0.027	0.026	0.010	0.004	0.001	0.019	0.012	0.007	0.004
5272	63.0	3	0	+1.689	+1.239	+0.684	+0.658	+0.430	+0.167	-0.196	-0.293	-0.422
				0.010	0.015	0.010	0.010	0.005	0.007	0.008	0.015	0.004
5904	63.0	4	0	+1.745	+1.289	+0.720	+0.691	+0.441	+0.190	-0.200	-0.317	-0.448
				0.021	0.013	0.008	0.012	0.010	0.007	0.013	0.011	0.012
6205	63.0	4	0	+1.671	+1.240	+0.695	+0.666	+0.439	+0.164	-0.198	-0.300	-0.427
				0.020	0.016	0.013	0.017	0.011	0.003	0.007	0.012	0.013
6254	63.0	3	0	+2.105	+1.629	+1.012	+0.965	+0.653	+0.275	-0.264	-0.481	-0.698
				0.006	0.010	0.025	0.030	0.019	0.006	0.016	0.021	0.024
6341	63.0	5	0	+1.583	+1.095	+0.610	+0.577	+0.401	+0.135	-0.197	-0.286	-0.412
				0.013	0.005	0.007	0.010	0.010	0.004	0.012	0.003	0.002
6356	63.0	4	0	+2.636	+2.266	+1.386	+1.298	+0.839	+0.397	-0.275	-0.538	-0.836
				0.023	0.010	0.012	0.015	0.027	0.013	0.014	0.006	0.011
6779	63.0	5	0	+2.079	+1.469	+0.906	+0.857	+0.601	+0.215	-0.277	-0.428	-0.618
				0.033	0.016	0.017	0.016	0.019	0.011	0.007	0.006	0.009
7078	63.0	3	0	+1.665	+1.156	+0.670	+0.629	+0.427	+0.123	-0.211	-0.319	-0.461
				0.024	0.022	0.022	0.022	0.019	0.014	0.014	0.015	0.015
7089	63.0	3	0	+1.674	+1.211	+0.706	+0.662	+0.447	+0.178	-0.182	-0.306	-0.437
				0.006	0.006	0.005	0.029	0.025	0.016	0.012	0.000	0.006

* Small diaphragm because of nearby star.

TABLE 4

PHOTOMETRIC ERRORS CAUSED BY REDSHIFT WHEN $(v_g - v_f) = 1500$ km s^{-1}

COLOR INDEX	ERROR	
	Observed (mag)	Predicted (mag)
(38 − 55).....	−0.024 ± 0.005	−0.040
(41 − 55).....	+0.007 ± 0.010	−0.007
(42 − 55).....	+0.035 ± 0.008	+0.020
(45 − 55).....	+0.035 ± 0.006	+0.030
(52 − 55).....	−0.035 ± 0.007	−0.040
(62 − 55).....	−0.007 ± 0.008	−0.010

curve. The coefficients $K_{(x-55)}$ for all colors, corresponding to a reddening excess of 0.05 mag in $B - V$, are shown in table 5. Colors corrected for both redshift and reddening will be denoted $(x - 55)_0$ to distinguish them from the uncorrected data in table 3. These corrected colors appear in table 6.

The values of $E(B - V)$ assumed in order to correct the colors of globular clusters for reddening, together with the sources of $E(B - V)$, are shown in table 7. Since the reddening for NGC 6356 seemed quite uncertain, corrected colors were computed for two extreme values, $E(B - V)$ equal to 0.30 and 0.50 mag. Table 8 presents the rms error of observation in each color computed from the internal mean errors for all the galaxies and globular clusters in table 3. Mean errors for clusters and galaxies are similar.

M31 and its two companions, M32 and NGC 205, form a group that meets all the criteria for group membership discussed above, and colors for all three on both the DDO and Wood systems have been published. Accordingly, colors were first trans-

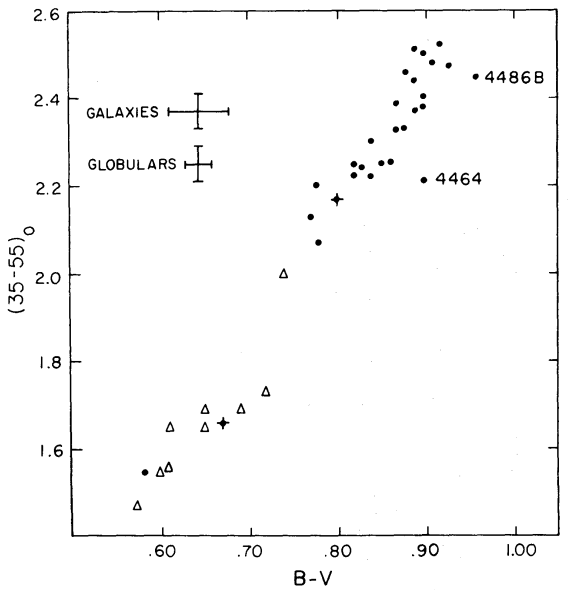

FIG. 1.—$(35 - 55)_0$ versus $B - V$ for galaxies (*dots*) and globular clusters (*triangles*). The two crosses represent M32 and NGC 205.

TABLE 5

COEFFICIENTS IN THE GALACTIC REDDENING LAW

$K_{(35-55)}$	+0.080	$K_{(52-55)}$	+0.013
$K_{(38-55)}$	+0.061	K_{55}	+0.150
$K_{(41-55)}$	+0.050	$K_{(62-55)}$	−0.017
$K_{(42-55)}$	+0.048	$K_{(67-55)}$	−0.028
$K_{(45-55)}$	+0.038	$K_{(74-55)}$	−0.039

formed to the photometric system in this paper by means of transformation equations derived from stellar data (Faber 1971, 1973*a*), and were then corrected for reddening and redshift. The transformed colors for all three galaxies have estimated mean errors of 0.05 mag. In all plots, these objects are represented by crosses in order to distinguish them from the galaxies observed in this study.

TABLE 6

GALAXY COLORS CORRECTED FOR REDDENING AND REDSHIFT AND CLUSTER COLORS CORRECTED FOR REDDENING

Name NGC	A/D_0	$(35-55)_0$ (mag)	$(38-55)_0$ (mag)	$(41-55)_0$ (mag)	$(42-55)_0$ (mag)	$(45-55)_0$ (mag)	$(52-55)_0$ (mag)	$(62-55)_0$ (mag)	$(67-55)_0$ (mag)	$(74-55)_0$ (mag)	$(LB)_0$ (mag)	$(CN)_0$ (mag)	$(G)_0$ (mag)	$(Mg)_0$ (mag)	$(TiO)_0$ (mag)
205	0.13*	+1.66	+1.26	+0.63	+0.60	+0.37	+0.23	−0.15	−0.28	−0.51	−0.10	+0.03	+0.23	−0.09	−0.01
221	0.21*	+2.17	+1.95	+1.08	+1.02	+0.53	+0.31	−0.19	−0.33	−0.49	−0.31	+0.06	+0.49	−0.11	+0.00
224	†	+2.52	+2.32	+1.34	+1.16	+0.60	+0.37	−0.20	−0.37	−0.58	−0.38	+0.18	+0.56	−0.15	−0.01
584	0.31	+2.304	+2.037	+1.149	+1.015	+0.558	+0.341	−0.207	−0.370	−0.605	−0.301	+0.134	+0.457	−0.133	−0.009
596	0.49	+2.204	+1.904	+1.046	+0.961	+0.531	+0.305	−0.181	−0.353	−0.560	−0.270	+0.085	+0.430	−0.107	−0.025
1332	0.27	+2.459	+2.177	+1.253	+1.098	+0.589	+0.371	−0.203	−0.392	−0.631	−0.311	+0.155	+0.509	−0.151	−0.026
1889	0.57	+2.131	+1.776	+1.022	+0.885	+0.486	+0.269	−0.228	−0.352	−0.551	−0.191	+0.137	+0.399	−0.088	+0.022
2300	0.69	+2.504	+2.195	+1.301	+1.118	+0.617	+0.374	−0.240	−0.414	−0.689	−0.283	+0.183	+0.501	−0.144	−0.002
2634	0.63	+2.191	+1.935	+1.078	+0.961	+0.504	+0.315	−0.151	−0.348	−0.555	−0.291	+0.117	+0.457	−0.127	−0.052
2672	0.53	+2.386	+2.048	+1.124	+1.002	+0.541	+0.349	−0.222	−0.383	−0.586	−0.283	+0.122	+0.461	−0.147	−0.002
2872	0.47	+2.373	+2.130	+1.185	+1.050	+0.542	+0.352	−0.187	−0.373	−0.604	−0.341	+0.135	+0.508	−0.150	−0.031
3073	0.34	+1.550	+1.157	+0.479	+0.380	+0.226	+0.128	−0.152	−0.284	−0.376	−0.134	+0.099‖	+0.154	−0.044	−0.014
3193	0.57	+2.221	+1.950	+1.097	+1.005	+0.543	+0.311	−0.206	−0.356	−0.593	−0.282	+0.092	+0.462	−0.108	−0.002
3226	0.59	+2.236	+1.843	+1.092	+0.982	+0.562	+0.291	−0.213	−0.390	−0.626	−0.170	+0.110	+0.420	−0.081	−0.015
3379	0.42	+2.334	+2.082	+1.168	+1.040	+0.553	+0.332	−0.223	−0.376	−0.635	−0.322	+0.128	+0.487	−0.126	+0.003
3605	0.79	+2.090	+1.800	+0.965	+0.907	+0.459	+0.250	−0.192	−0.327	−0.544	−0.263	+0.058	+0.448	−0.079	+0.001
3608	0.74	+2.255	+1.983	+1.080	+0.989	+0.537	+0.303	−0.205	−0.362	−0.599	−0.306	+0.091	+0.452	−0.103	−0.006
3613	0.46	+2.240	+1.972	+1.079	+0.969	+0.499	+0.303	−0.201	−0.360	−0.564	−0.303	+0.110	+0.470	−0.117	−0.009
4261	0.50	+2.313	+2.149	+1.218	+1.062	+0.550	+0.360	−0.193	−0.375	−0.614	−0.344	+0.156	+0.512	−0.155	−0.026
4278	0.54	+2.330	+1.987	+1.158	+1.062	+0.570	+0.346	−0.218	−0.401	−0.662	−0.234	+0.096	+0.492	−0.133	−0.016
4283	0.76	+2.256	+1.971	+1.099	+1.012	+0.545	+0.293	−0.171	−0.373	−0.615	−0.284	+0.087	+0.467	−0.090	−0.047
4464	0.51	+2.209	+1.967	+1.098	+1.005	+0.549	+0.308	−0.164	−0.341	−0.570	−0.305	+0.093	+0.456	−0.103	−0.035
4472	0.23	+2.438	+2.162	+1.231	+1.091	+0.568	+0.368	−0.204	−0.386	−0.645	−0.318	+0.140	+0.523	−0.156	−0.021
4478	0.21	+2.255	+1.966	+1.091	+1.013	+0.549	+0.329	−0.189	−0.361	−0.589	−0.284	+0.078	+0.464	−0.124	−0.022
4486	0.29	+2.404	+2.140	+1.253	+1.096	+0.580	+0.385	−0.195	−0.398	−0.651	−0.302	+0.157	+0.516	−0.169	−0.037
4486B	1.14	+2.419	+2.132	+1.213	+1.090	+0.585	+0.343	−0.200	−0.375	−0.607	−0.306	+0.123	+0.505	−0.125	−0.019
4627	0.46	+1.606	+1.090	+0.462	+0.431	+0.253	+0.143	−0.079	−0.187	−0.226	−0.047	+0.031	+0.178	−0.049	−0.030
4649	0.30	+2.475	+2.207	+1.268	+1.104	+0.578	+0.358	−0.229	−0.406	−0.665	−0.326	+0.164	+0.526	−0.142	−0.008
5846	0.44	+2.507	+2.227	+1.264	+1.112	+0.604	+0.394	−0.207	−0.398	−0.659	−0.332	+0.152	+0.508	−0.169	−0.025
5846A	1.01	+2.376	+2.058	+1.164	+1.057	+0.567	+0.356	−0.217	−0.393	−0.623	−0.278	+0.107	+0.490	−0.144	−0.012
5982	0.79	+2.227	+1.969	+1.088	+0.946	+0.500	+0.305	−0.171	−0.330	−0.505	−0.302	+0.142	+0.446	−0.119	−0.022
6307	0.55	+2.173	+1.914	+1.038	+0.930	+0.502	+0.286	−0.201	−0.351	−0.528	−0.299	+0.108	+0.428	−0.099	−0.004
7619	0.78	+2.519	+2.184	+1.264	+1.112	+0.571	+0.367	−0.272	−0.432	−0.647	−0.282	+0.152	+0.541	−0.154	+0.020
7626	0.83	+2.503	+2.108	+1.206	+1.068	+0.560	+0.344	−0.242	−0.431	−0.648	−0.243	+0.138	+0.508	−0.135	−0.010
5024		+1.545	+1.105	+0.603	+0.570	+0.375	+0.121	−0.164	−0.257	−0.371	−0.023	+0.032	+0.195	+0.019	+0.013
5272		+1.688	+1.239	+0.684	+0.658	+0.430	+0.167	−0.196	−0.293	−0.422	−0.044	+0.026	+0.228	−0.006	+0.024
5904		+1.728	+1.276	+0.709	+0.681	+0.433	+0.187	−0.196	−0.311	−0.440	−0.049	+0.028	+0.248	−0.025	+0.014
6205		+1.646	+1.221	+0.679	+0.651	+0.427	+0.160	−0.192	−0.291	−0.415	−0.051	+0.028	+0.224	−0.001	+0.022
6254		+1.688	+1.311	+0.751	+0.715	+0.455	+0.207	−0.175	−0.335	−0.494	−0.084	+0.036	+0.260	−0.037	−0.021
6341		+1.550	+1.070	+0.589	+0.557	+0.385	+0.129	−0.190	−0.274	−0.396	−0.007	+0.032	+0.172	+0.015	+0.030
6356‡		+1.835	+1.655	+0.886	+0.817	+0.459	+0.267	−0.105	−0.258	−0.446	−0.287	+0.068	+0.359	−0.095	−0.046
6356§		+2.155	+1.899	+1.086	+1.009	+0.611	+0.319	−0.173	−0.370	−0.602	−0.270	+0.077	+0.398	−0.093	−0.045
6779		+1.647	+1.139	+0.636	+0.597	+0.395	+0.144	−0.185	−0.276	−0.407	+0.009	+0.038	+0.202	+0.003	+0.024
7078		+1.473	+1.009	+0.550	+0.513	+0.335	+0.091	−0.170	−0.251	−0.367	+0.009	+0.036	+0.178	+0.034	+0.023
7089		+1.546	+1.113	+0.626	+0.585	+0.386	+0.157	−0.154	−0.261	−0.374	−0.021	+0.040	+0.199	−0.013	+0.001

* Mean diaphragm size of 46" assumed. A = 40" (McClure and van den Bergh 1968b); 51" (Wood 1966).

† A = 17" (McClure and van den Bergh 1968b); 18" (Wood 1966).

‡ E (B-V) = 0.50 magnitude.

§ E (B-V) = 0.30 magnitude.

‖ Index may be affected by Hδ.

TABLE 7

REDDENING OF GLOBULAR CLUSTERS

Cluster (NGC)	$E(B-V)$ (mag)	Source(s)
5024.....	0.05	Hartwick (1968)
5272.....	0.00	Sandage (1969); McClure and Racine (1969)
5904.....	0.01	Arp (1962)
6205.....	0.015	Sandage (1969); McClure and Racine (1969)
6254.....	0.26	Sandage (1969)
6341.....	0.02	Hartwick (1968)
6356.....	0.50	Sandage and Wallerstein (1960);
	0.38	Hartwick (1968)
6779.....	0.27	Hartwick (1968)
7078.....	0.12	Sandage (1969)
7089.....	0.08	Hartwick (1968)

In figure 1, $(35-55)_0$ is compared to $B-V$ for galaxies and globular clusters. Values of $B-V$, corresponding to an aperture D_0 and corrected for the effects of redshift and galactic reddening, were taken from the RCBG, where they are called C_0. Values of $B-V$ given by van den Bergh (1967) and corrected in accordance with the color excesses in table 7 have been used to locate globular clusters (*triangles*) in the diagram. The graph demonstrates that differences in $(35-55)_0$ correspond closely to differences in integrated $B-V$ even though the values of $(35-55)_0$ generally were measured with aperture sizes smaller than D_0.

V. COLOR-COLOR AND COLOR-MAGNITUDE DIAGRAMS

With this 10-color system one can form five photometric indices that are useful indicators of the strengths of absorption due to CN, the G band, Mg "b" plus MgH, TiO, and metallic-line blanketing near 3800 Å [denoted by $(LB)_0$]. Following McClure and van den Bergh (1968*b*), we have taken the CN index as $(41-42)$ and the G-band index as $(42-45)$. The other three indices correspond to the difference between the magnitude measured in the absorption feature and the magnitude interpolated between neighboring "continuum" points (fig. 2). Thus the indices $(LB)_0$, $(Mg)_0$, and $(TiO)_0$ correspond to the magnitude difference $M_D - M_B$ shown in figure 2. With these definitions, the following expressions for the absorption-line indices result:

$$\begin{aligned}
(CN)_0 &= (41-42)_0\,, \\
(G)_0 &= (42-45)_0\,, \\
(LB)_0 &= 0.492(41-55)_0 + 0.508(35-55)_0 - (38-55)_0\,, \\
(Mg)_0 &= 0.373(45-55)_0 - (52-55)_0\,, \\
(TiO)_0 &= 0.584(67-55)_0 - (62-55)_0\,. \qquad (1)
\end{aligned}$$

Table 8 presents the mean error of observation associated with each index. $(CN)_0$ and $(G)_0$ increase with increasing line absorption, while the other three indices decrease.

In figure 3, values of the line indices, along with the three continuum colors $(45-55)_0$, $(67-55)_0$, and $(74-55)_0$, are plotted against $(35-55)_0$. The strengths of the absorption indices $(LB)_0$, $(CN)_0$, and $(Mg)_0$ clearly increase monotonically with

TABLE 8

INTERNAL MEAN ERRORS OF GALAXY AND CLUSTER OBSERVATIONS

Index	Error (mag)	Index	Error (mag)
(35 − 55).....	0.018	(74 − 55).....	0.014
(38 − 55).....	0.021	$(LB)_0$.....	0.020
(41 − 55).....	0.017	$(CN)_0$.....	0.016
(42 − 55).....	0.017	$(G)_0$.....	0.015
(45 − 55).....	0.014	$(Mg)_0$.....	0.013
(52 − 55).....	0.012	$(TiO)_0$.....	0.013
(62 − 55).....	0.015	$(CN + Mg)_0$.....	0.020
(67 − 55).....	0.011		

increasing continuum color. NGC 6356 has been plotted twice in accordance with the two values of the reddening excess used to correct the colors. Hence in each figure the line connecting the two points for NGC 6356 represents a reddening vector with length 0.20 mag in $E(B - V)$.

Figure 4*a* presents a color-magnitude diagram for these elliptical galaxies. The absolute visual magnitudes, M_V, are based on mean group radial velocities together with a Hubble constant of 95 km s^{-1} Mpc^{-1} (van den Bergh 1970). Van den Bergh (1960) has suggested that the pair of galaxies NGC 4627, 4631 are members of the Canes Venatici cluster. Since the velocity of NGC 4631 differs considerably from the cluster velocity, 4627 is plotted twice according to the two resultant values of the distance.

Figure 4*a* shows a rapid decline in the $(35 - 55)_0$ index at an absolute magnitude near −16.5. In this regard, the diagram resembles one presented by Baum (1959). However, above the point $M_V = -17$, the color index continues to increase slowly as a function of intrinsic luminosity. Although substantiated by the data as a whole, this trend is most clearly delineated by the slopes of lines joining members of the same pair. These slopes are unaffected by errors in the galactic reddening corrections and by errors in M_V caused by scatter about the redshift-distance relation. Therefore they provide a measure of the slope of the relation that is essentially free of systematic error.

VI. ANALYSIS INTO PRINCIPAL COMPONENTS

Although figures 3 and 4*a* indicate that the colors, line strengths, and absolute magnitudes of elliptical galaxies are highly correlated, the scatter in many of these

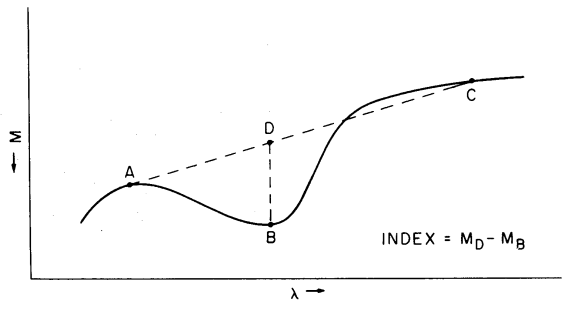

FIG. 2.—An idealized section of a galaxy spectrum containing a broad absorption feature. The indices $(LB)_0$, $(Mg)_0$, and $(TiO)_0$ correspond to the difference in magnitudes between points *D* and *B*.

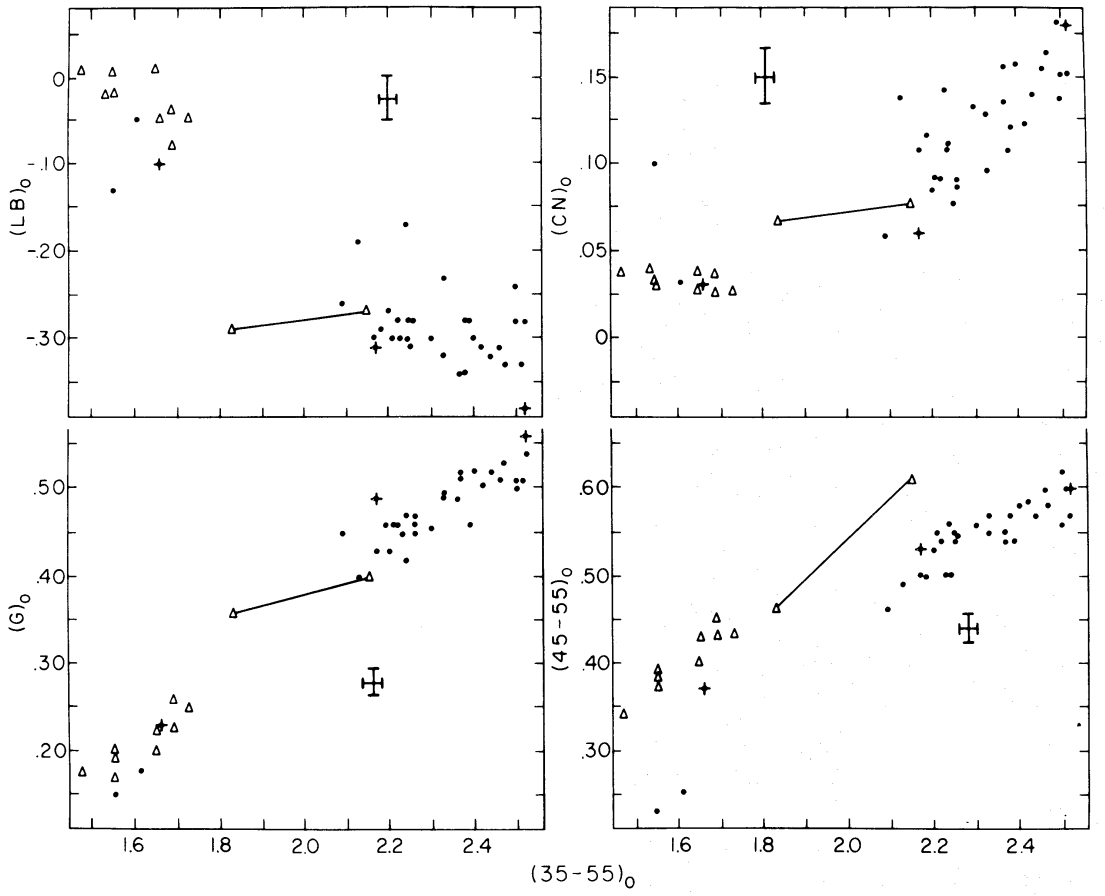

FIG. 3*a*.—Line indices and continuum colors as a function of $(35 - 55)_0$ for elliptical galaxies (*dots*) and globular clusters (*triangles*). Crosses represent M31, M32, and NGC 205. NGC 6356 is plotted twice according to the two values assumed for the reddening excess, $E(B - V) = 0.30$ and 0.50 mag.

plots exceeds the scatter to be expected from observational errors alone. This dispersion in photometric properties could conceivably arise from variations in one or more physical parameters other than absolute magnitude. Principal component analysis is a statistical technique that can explore this possibility in a systematic way. Deeming (1964) has used it to classify 5-color photometry for late-type giant stars, and Martin and Bingham (1970) have applied it to Wood's 12-color measures on galaxies. The reader is referred to these papers and to Kendall and Stuart (1966) for a fundamental discussion of the method.

A 10-color photometric system provides nine independent color indices for each object observed. Each object can therefore be represented as a point in a nine-dimensional space. We wish to find the number of dimensions in the subspace occupied by these elliptical galaxies. The number of dimensions in this subspace equals the number of independent parameters necessary to specify exactly the colors of a given elliptical galaxy. Because of observational errors alone, these galaxies in reality fill a nine-dimensional volume. But the width of the space in certain directions may be due purely to observational scatter, in which case this variation would not signify the need for an additional independent descriptive parameter. Therefore, a method that yields the number of dimensions in the subspace should also indicate whether the width in

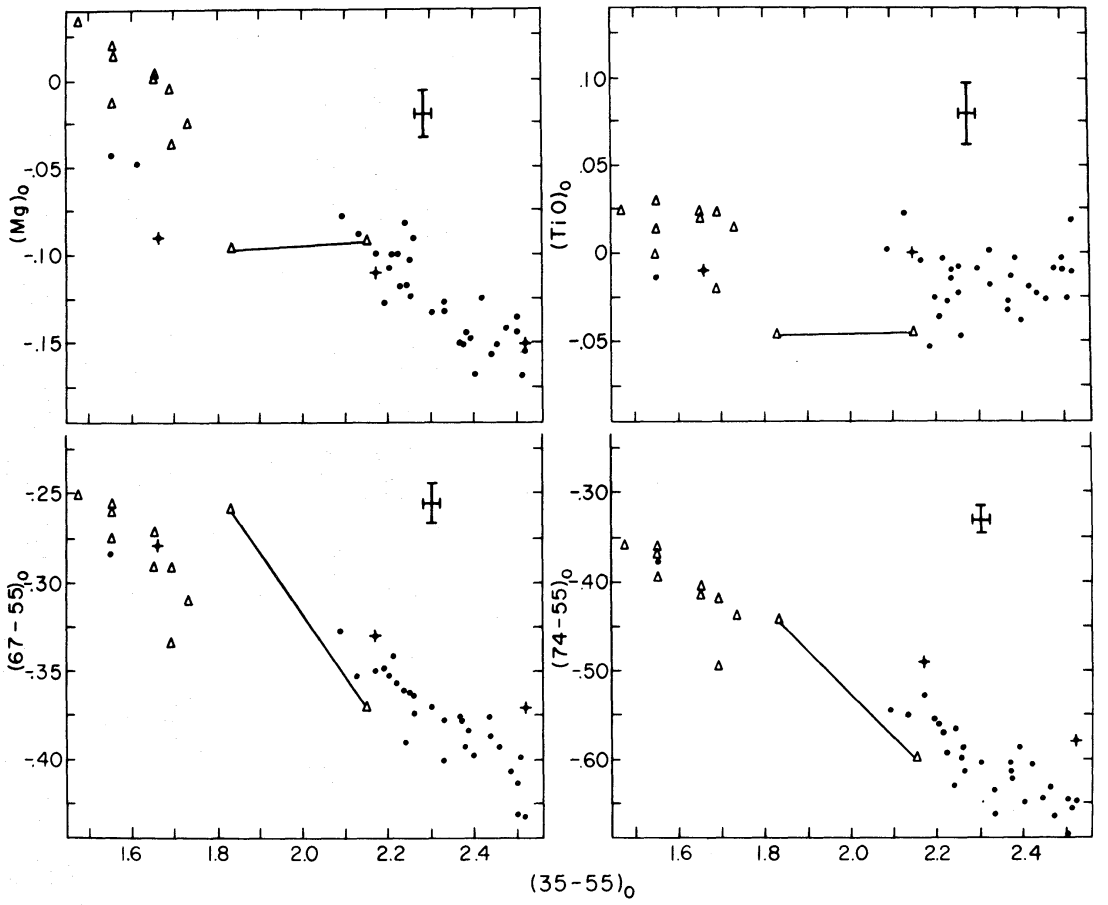

FIG. 3*b*.—Same as fig. 3*a*

certain directions has statistical significance, given the observational errors in the original quantities. We also require expressions for the linearly independent parameters needed to specify uniquely the position of an object in the space. In the case of the elliptical galaxies, for example, the discussion above suggests that at least one of these parameters is closely correlated with absolute magnitude.

Suppose that the original n-dimensional variables have been transformed to ones having zero mean and unit variance. The method of principal component analysis yields a set of n orthogonal vectors, $\boldsymbol{v}_i$, called principal components. The vector $\boldsymbol{v}_1$ is the direction along which the variance is maximized. The remaining variance is maximized along direction $\boldsymbol{v}_2$, and so on. We define a quantity $K_{ij} \equiv \boldsymbol{v}_i \cdot \boldsymbol{x}_j$, where $\boldsymbol{x}_j$ is the position of object j in the space. Then the variance λ_i associated with $\boldsymbol{v}_i$ is $\sum K_{ij}^2/N$, where N is the total number of objects in the sample. Let Q_i represent the expected value of the variance along $\boldsymbol{v}_i$ due to observational errors alone. If the mean error of observation associated with each coordinate m is δx_m, then

$$Q_i = \sum_{lm} \sum v_{il} v_{im} \langle \delta x_l \delta x_m \rangle \,. \tag{2}$$

Here $\langle \delta x_l \delta x_m \rangle$ is the covariance between variables x_l and x_m. If λ_i is much larger than Q_i, the variance along $\boldsymbol{v}_i$ is much larger than can be explained by errors alone and must have physical significance. According to Deeming (1964) the quantity λ_i/Q_i

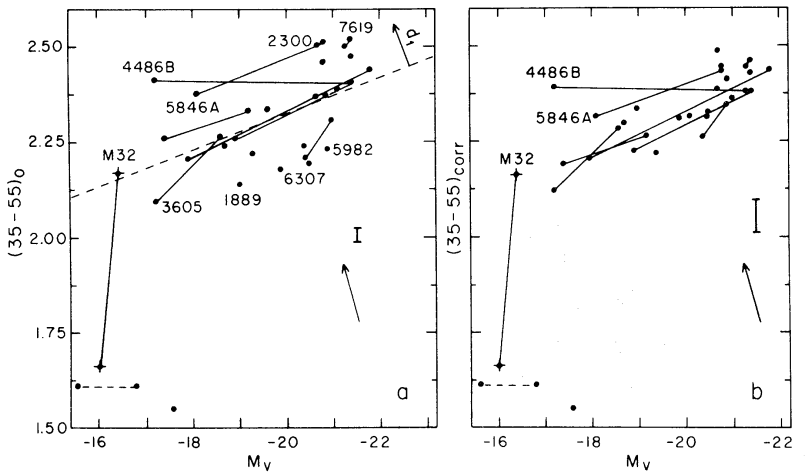

FIG. 4*a* (*left*).—Color-magnitude diagram for elliptical galaxies. The ordinates are values of $(35 - 55)_0$ from table 6. Straight lines connect members of the same pair. The dashed line represents the linear least-squares relation for the upper group of points. NGC 4627 has been plotted twice (points connected by dashed line) according to two different values of the distance modulus. Crosses represent M32 and NGC 205. The arrow is a reddening vector of length 0.10 mag in $E(B - V)$.

FIG. 4*b* (*right*).—Same as fig. 4*a* except $(35 - 55)_{corr}$, corrected for residual reddening errors, is used as ordinate.

follows the F distribution with $(N - 1)$ degrees of freedom. This fact provides a convenient statistical test for the significance of λ_i.

As the nine independent variables x_{jm}, the solutions utilized the four continuum color indices plus the five line indices, suitably translated to the origin and normalized to unit variance as described above. These variables were assigned to the coordinate axes as described in table 9. For example, x_{j3} indicates the $(CN)_0$ index, translated and normalized, for the jth object in table 6.

Table 10 presents the values of the variances λ_i, the expected variances Q_i, the ratio λ_i/Q_i, and the components of the vectors $\boldsymbol{v}_i$ for the solution treating all the galaxy data. Tables of percentage points for the F distribution show that λ_1, λ_2, λ_3, and λ_4 are significantly greater than Q_1, Q_2, Q_3, and Q_4 at the 0.5 percent confidence level. The remaining variances are not significant. The significance level ascribed to a given λ_i is a rapidly changing function of the ratio λ_i/Q_i in the range 2.0 to 3.0. Therefore, one should test for the stability of the solution and the accuracy of the ratios λ_i/Q_i by repeating the analysis into principal components using subsets of the original data. If the vectors $\boldsymbol{v}_i$ and variances λ_i remain fairly constant during these trials, the significance estimates are not unstable with respect to minor alterations in the data.

TABLE 9

COORDINATES FOR THE ANALYSIS INTO PRINCIPAL COMPONENTS

Coordinate	Index	Coordinate	Index
x_{j1}	$(35 - 55)_0$	x_{j6}	$(Mg)_0$
x_{j2}	$(LB)_0$	x_{j7}	$(TiO)_0$
x_{j3}	$(CN)_0$	x_{j8}	$(67 - 55)_0$
x_{j4}	$(G)_0$	x_{j9}	$(74 - 55)_0$
x_{j5}	$(45 - 55)_0$		

1973ApJ...179..731F

TABLE 10

ANALYSIS INTO PRINCIPAL COMPONENTS: ALL GALAXIES

i	λ_i	Q_i	λ_i/Q_i	v_{i1}	v_{i2}	v_{i3}	v_{i4}	v_{i5}	v_{i6}	v_{i7}	v_{i8}	v_{i9}
1.....	6.560	0.033	197.00	+0.383	−0.327	+0.301	+0.374	+0.372	−0.344	+0.021	−0.361	−0.355
2.....	0.515	0.172	2.98	−0.018	+0.088	+0.849	−0.231	−0.306	−0.250	−0.023	+0.058	+0.237
3.....	0.434	0.137	3.16	−0.028	+0.692	+0.028	−0.244	+0.044	+0.005	−0.280	−0.408	−0.460
4.....	0.122	0.043	2.80	+0.461	+0.512	+0.067	+0.303	+0.376	+0.135	−0.032	+0.177	+0.484
5.....	0.011	0.010	1.03	−0.754	+0.070	+0.100	+0.319	+0.343	−0.082	−0.006	−0.313	+0.301
6.....	0.022	0.027	0.81	+0.156	−0.220	−0.113	−0.695	+0.396	−0.048	+0.008	−0.362	+0.373
7.....	0.215	0.149	1.43	+0.008	−0.223	+0.345	+0.031	+0.067	+0.878	−0.141	−0.162	−0.086
8.....	1.064	0.641	1.67	+0.009	+0.200	+0.064	−0.044	−0.024	+0.139	+0.945	−0.174	−0.095
9.....	0.060	0.047	1.25	−0.211	+0.014	+0.188	−0.257	+0.585	−0.013	+0.069	+0.617	−0.351

Several subsets of the galaxy data were chosen for this purpose. The tests showed that vectors v_3 and v_4 varied appreciably and the significance levels for both λ_3 and λ_4 fell below 5 or 10 percent unless the data for M31, M32, and NGC 205 were included. Since the colors for these objects are of lower reliability, it is doubtful that vectors v_3 and v_4 are physically meaningful. Furthermore, the principal contributor to both vectors v_3 and v_4 is the index $(LB)_0$, which measures the line blanketing in filter 38. This filter is fairly narrow and lies in a region of the spectrum where intensities change rapidly over a few angstroms. For this reason, measurements through this filter are especially sensitive to redshift errors. As a final check on the solution, index $(LB)_0$ was eliminated and the remaining eight indices analyzed into principal components. Only two significant vectors appeared, corresponding to v_1 and v_2. Both were significant to the 0.5 percent confidence level. We therefore conclude that the evidence for additional components v_3 and v_4 lies exclusively in the index $(LB)_0$. Since this is the least reliable color index, the reality of v_3 and v_4 is doubtful.

On the other hand, both v_1 and v_2 have obvious mathematical significance. The parameter K_{1j} can be described as the *sum* of the continuum colors plus absorption-line strengths, whereas K_{2j} is the *difference* between the continuum colors and the two principal absorption indices $(CN)_0$ and $(Mg)_0$. K_{2j} is plotted versus K_{1j} in figure 5. Aside from the 3 bluest galaxies, NGC 205, 3073, and 4627, the remainder of the points fill a cigar-shaped region in the diagram. This group will henceforth be referred to as the "redder" group. A few of the points on the outer edge of the cigar have been labeled. Comparison of figure 5 with the color-magnitude diagram in figure 4*a* shows that points that lie on the outer edges of the distribution in figure 5 also do so in figure 4*a*. Figure 6 displays this correlation graphically. The distance (d_1) of an object from the least-squares line drawn in figure 4*a* has been plotted against its distance (d_2) from the line drawn in figure 5. (The line in fig. 5 was drawn by eye to correspond as closely as possible to the least-squares line in fig. 4*a*.) The vectors drawn in figures 5 and 6

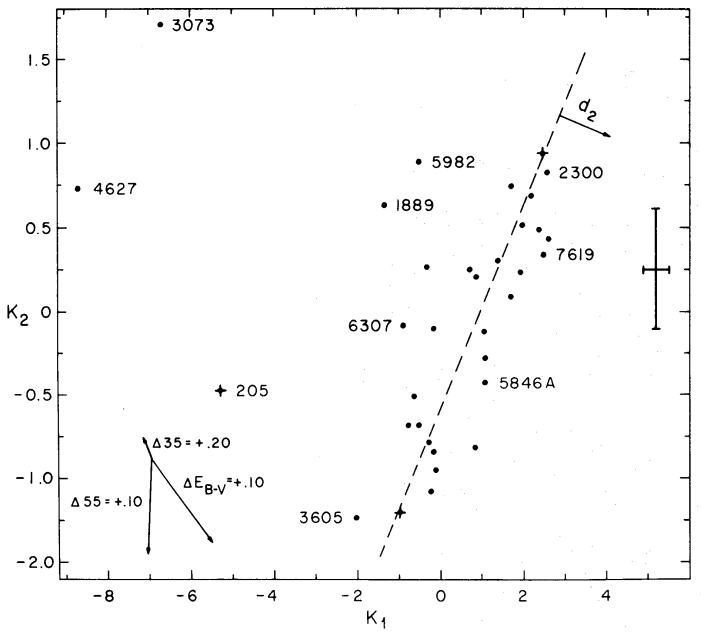

FIG. 5.—K_1 versus K_2. The dashed line corresponds to the dashed line in fig. 4*a*. The vectors indicate the effects of errors in filters 35 and 55 and in the assumed reddening. Crosses represent M31, M32, and NGC 205.

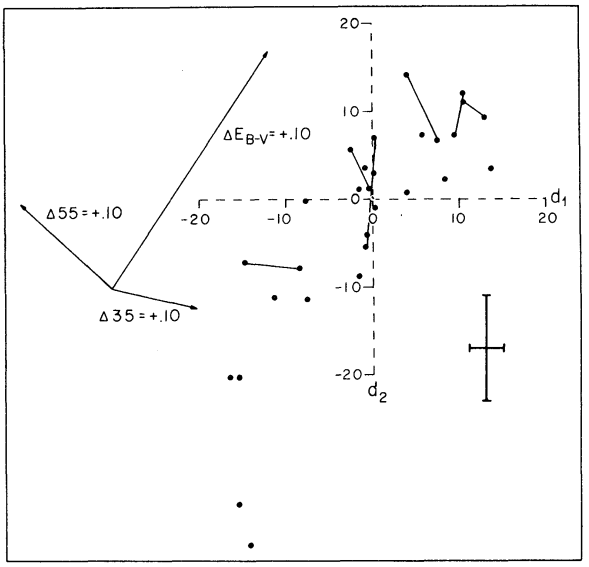

FIG. 6.—The distance d_1 (fig. 4*a*) versus the distance d_2 (fig. 5). Straight lines connect members of the same pair. The vectors indicate the effects of errors in filters 35 and 55 and in the assumed reddening.

represent the effects on K_{ij}, K_{2j}, d_1, and d_2 of observational errors in magnitudes 35 and 55. These vectors demonstrate that the correlation between d_1 and d_2 is not due simply to errors in the observations in filters 35 or 55. On the other hand, the reddening vector in figure 6 shows that errors of less than 0.10 mag in the reddening estimates $E(B - V)$ are sufficient to cause most of the variance in d_1 and d_2. Deviations from the mean lines in figures 4*a* and 5 are generally parallel to the reddening vectors in those figures also. Therefore, residual reddening errors seem a likely cause of the correlated residuals d_1 and d_2. Further evidence supporting this conclusion is presented below.

In figure 7 the sum of the $(CN)_0$ and $(Mg)_0$ indices [actually $(CN)_0 - (Mg)_0$] is plotted versus absolute magnitude for the elliptical galaxies. In a separate paper

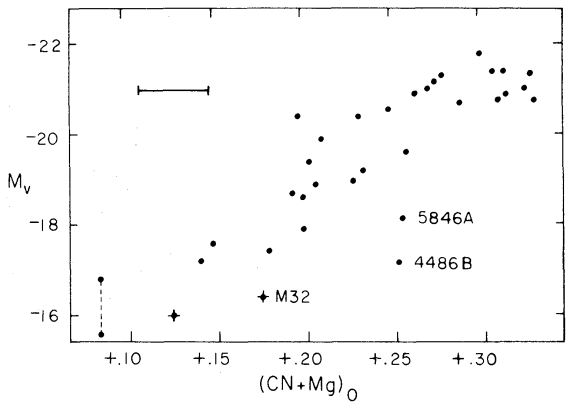

FIG. 7.—The line index $(CN + Mg)_0$ as a function of absolute magnitude for elliptical galaxies. NGC 4627 is plotted twice (two points connected by dashed line). The three labeled points are discussed in the text. Crosses represent M32 and NGC 205.

(Faber 1973*b*) we show that on the basis of colors, line strengths, and surface brightness, the three galaxies M32, NGC 4486 B, and NGC 5846 A are anomalous objects. Several lines of argument suggest that these galaxies are in fact remnants of tidal encounters with more massive companion galaxies. If these three points are ignored, figure 7 shows that the integrated line strength of elliptical galaxies in the $(CN)_0$ and $(Mg)_0$ indices is a monotonically increasing function of absolute magnitude. The scatter in the diagram is comparable to that expected from observational errors alone. The standard deviation in M_V about a least-squares cubic fit to the points in figure 7 (M32, NGC 4486 B, and NGC 5846 A omitted) is 0.56 mag. Since this composite index is virtually unaffected by errors in the reddening correction, for these elliptical galaxies $(CN + Mg)_0$ is a reddening-free indicator of absolute magnitude with an accuracy of ± 0.56 mag. The sense of the correlation is in accord with the suggestion by McClure and van den Bergh (1968*b*) that CN is weaker in dwarf elliptical galaxies. The increase in line strength with increasing luminosity found here also agrees with their result (McClure and van den Bergh 1968*a*) that the metallicity index Q increases with luminosity. However, the index $(CN + Mg)_0$ appears to be nearly twice as accurate as Q in predicting M_V.

This close correlation between line strength and luminosity further supports the conclusion that errors in the reddening correction are the cause of the scatter in figures 4*a* and 5. If reddening is rejected as the cause of scatter and the deviations in the figures are taken to represent features intrinsic to the spectra of these galaxies, we reach the implausible conclusion that the line strengths of elliptical galaxies are very closely correlated with absolute magnitude while continuum colors are much less closely correlated. Reddening errors provide a much more attractive explanation, and in the ensuing discussion, reddening will be accepted as the cause of scatter.

Approximate corrections to $(35 - 55)_0$ for the redder galaxies can be derived if the distance of a point from the line drawn in figure 5 is taken as a measure of the error in reddening associated with each object. In no case, however, should a "dereddening" correction be used that exceeds the original correction applied. Plots of M_V and $(CN + Mg)_0$ versus this corrected index (figs. 4*b* and 8) do indeed have markedly less scatter than before.

Thus far, the location of the reddening medium has not been specified. If the reddening variations are intrinsic to our Galaxy or entire groups of galaxies, however, the deviations d_1 and d_2 should be similar for members of the same pair. Figure 6 indicates that this is true. In this diagram, pair members, connected by straight lines, tend to lie within similar regions of the sequence. This result suggests that within the accuracy attained in the present study, reddening errors for pair members are equal. Hence, reddening intrinsic to individual ellipticals is probably small.

Since the galaxy colors were originally corrected for reddening by means of the cosecant law, the presence of residual reddening errors indicates that the cosecant law is sometimes inaccurate. A plot of the reddening corrections $\triangle(35 - 55)_0$ versus the absolute value of the galactic latitude (fig. 9) tests the correctness of the coefficient in the cosecant law. A positive correction indicates that the absorption is less than that predicted by the cosecant law. Since no systematic trend with galactic latitude is well established, these data do not conflict with a coefficient of 0.05 magnitude for $E(B - V)$ in the cosecant correction.

On the other hand, figure 9 does suggest that local variations about a mean reddening law can be considerable. The present data indicate that elliptical galaxies can be a useful tool in mapping absorption as a function of position in our Galaxy and along the line of sight in intergalactic space. The ultimate accuracy of the method depends only on how closely correlated the integrated continuum colors and line strengths in elliptical galaxies actually are. We stress in this connection that in all probability only two independent parameters K_{1j} and K_{2j} are required to specify completely the colors

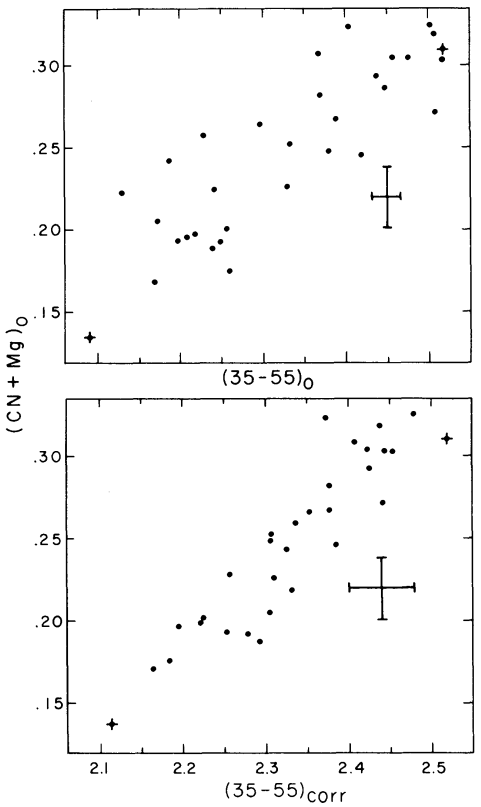

FIG. 8.—The line index (CN + Mg)$_0$ versus (35 − 55)$_0$ and (35 − 55)$_{corr}$, corrected for residual reddening errors. The three bluest galaxies, NGC 205, 3073, and 4627, are omitted. Crosses represent M31 and M32.

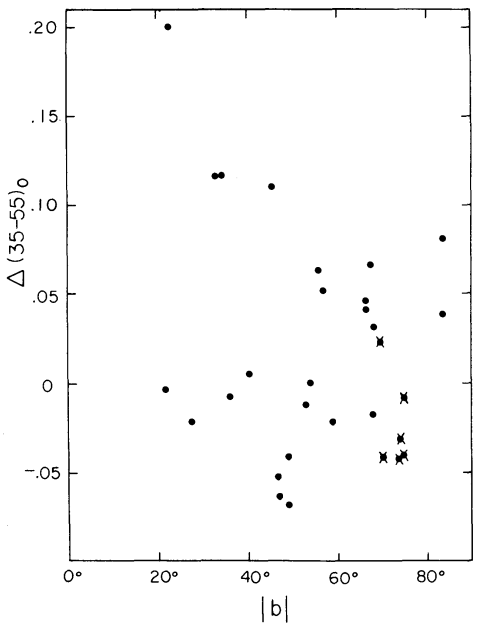

FIG. 9.—Residual reddening corrections, △(35 − 55), as a function of the absolute value of the galactic latitude. Crosses represent members of the Virgo cluster.

of the elliptical galaxies in this sample. These two parameters in turn yield the true colors of the galaxies and the residual reddening corrections. Figure 8 shows that the correlation between the corrected color $(35 - 55)_{corr}$ and the line strength is nearly perfect to within the accuracy of these data. Therefore, this study suggests that the integrated continuum colors and line strengths of elliptical galaxies are indeed precisely correlated. With the photometric accuracy achieved here, reddening can be determined to within ± 0.02 mag in $E(B - V)$.

It is important to verify that the correlations found in this study between absolute magnitude and integrated color and line strength do not result from systematic error. Residual uncorrected errors due to redshift are much too small to produce the effect. However, a systematic variation in A/D_0 with luminosity might possibly create a spurious correlation because the colors and line strengths of elliptical galaxies are known to vary systematically as a function of distance from the nucleus. We have checked for such a dependence of A/D_0 on M_V and also estimated the corrections to colors and line strengths arising from the use of apertures smaller than D_0. Both procedures confirm that the correlation between color and absolute magnitude is real and not due to systematic error. Furthermore, figure 1 demonstrates that the values of $(35 - 55)_0$ measured in this paper correlate well with integrated values of C_0. This fact is additional evidence that the observed change in color with absolute magnitude reflects a real change in the integrated properties of the galaxies as a function of luminosity.

VII. DISCUSSION

The present data indicate that, to a high degree of accuracy, the integrated colors and line strengths of a normal elliptical galaxy are determined by its absolute magnitude. However, in an effort to examine whether pair membership, cluster membership, and line or radio emission correlate with elliptical-galaxy colors, a search was made for relationships between these parameters, galaxy luminosity, and isolated color anomalies. The following paragraphs summarize the results of this search.

Galaxies in this study having line or radio emission (table 11) have colors that are completely normal for their absolute magnitudes. This fact suggests that the integrated stellar content of these galaxies is largely unrelated to the phenomena responsible for the line or radio emission. King (1971) has expressed the similar opinion that nuclear activity has little effect on stellar content. If this conclusion is generally true, the

TABLE 11

GALAXIES HAVING RADIO SOURCES OR EMISSION LINES

NGC No.	Emission		Reference(s)
	Radio	λ3727	
584.....	Ident. uncertain	...	Mills, Slee, and Hill (1958) Minkowski (1961) Heeschen and Wade (1964) Rogstad and Ekers (1969)
3226.....	...	Yes	Burbidge and Burbidge (1965)
4261.....	Yes	...	Minkowski (1961)
4278.....	Yes	Yes	Osterbrock (1960) Heeschen and Wade (1964) Rogstad and Ekers (1969)
4472.....	Yes	...	Heeschen and Wade (1964)
4486.....	Virgo A	Yes	Humason *et al.* (1956)
5846.....	...	Yes	Humason *et al.* (1956)
7626.....	Yes	...	Heeschen and Wade (1964)

peculiar colors of certain radio galaxies (for example, NGC 1275 and NGC 5128) must arise from nonstellar sources of emission or abnormal amounts of internal reddening.

Among the galaxies in the present sample, the only definitely abnormal object, NGC 3226 (through filter 38), is also the only companion of a Seyfert galaxy. Clearly, from a sample of one object no conclusions can be drawn concerning the possible relation between the components of the pair. Aside from M32, discussed above, the other interacting systems (NGC 1889, 2672, 3193, and 4627) are normal.

Finally, neither the colors nor the absolute magnitudes of any of the galaxies are related to the morphological types or number of companions. The colors of elliptical galaxies inside large clusters are identical to those of the same absolute magnitude in much smaller aggregates. Fish (1964) suggested that the mass-to-light ratio of elliptical galaxies with Sb or Sc companions was systematically low. All four of the galaxies cited by him—M32, NGC 2300, 3379, and 4649—were observed in this study. Aside from M32, which probably is a tidal remnant, no evidence was found that the colors of these galaxies are anomalous. (However, since photometric indices shortward of 8000 Å are not particularly sensitive to the mass-to-light ratio it is possible that variations in $\mathfrak{M}/L$ can go undetected in the photometric indices.) In summary, the integrated colors and line strengths of elliptical galaxies appear to be remarkably independent of all physical properties tested other than luminosity.

The three bluest galaxies in the present sample—NGC 205, 3073, and 4627—resemble globular clusters in having blue continua and weak absorption lines. These results support the findings of McClure and van den Bergh (1968*b*), Hodge (1971), and others, who have noted the similarities between globular clusters and dwarf ellipticals of low surface brightness. When all the elliptical galaxies studied here are ordered according to color, surface brightness, and metal abundance (see below), these three bluest clearly stand out as a separate group. Further photometric observations are clearly desirable to determine whether, in fact, transitional galaxies intermediate between the red and blue groups exist.

IX. THE RELATION BETWEEN GALAXY COLOR AND METAL ABUNDANCE

The monotonic change in integrated photometric indices with absolute magnitude suggests that one or more parameters characterizing the integrated stellar population varies systematically with galaxy luminosity. Models of the populations deduced from the integrated colors of these elliptical galaxies were presented in an earlier paper (Faber 1972). The galaxies were divided into five groups according to integrated color. Group 1, the bluest, contained the three blue dwarfs of low surface brightness. Not surprisingly, group 1 models strongly resembled globular clusters in our own galaxy. For the redder galaxies (groups 2 through 5), an increase in the number of strong-lined stars, together with a decrease in the light contributions from metal-poor objects, was necessary to duplicate the change in color and line strength with absolute magnitude. The mass-to-light ratios were indeterminate. Even though a few giants indicated by Spinrad and Taylor (1969) as super-metal-rich (SMR) were available for the synthesis, the line strengths in the computed models for the brightest galaxies (groups 4 and 5) were too weak.

The increase in the CN and Mg indices suggests that the mean metal abundance of the stellar population increases with luminosity in these ellipticals. Therefore, a rigorous attempt at population synthesis would utilize a complete grid of stellar colors of stars of different masses, ages, *and* composition. Unfortunately, one cannot determine the physical parameters of field stars with sufficient precision to fill this need. For this reason, the series of population models computed for groups 2 through 5 is not completely satisfactory.

In the absence of data for a complete set of stellar synthesis groups, one must adopt an indirect approach to this problem. For simplicity, a coeval population is assumed. The galaxy continuum colors depend strongly on both the age of the population (mass at turnoff from the main sequence) and the mean metal abundance. They are relatively insensitive to the luminosity function along the main sequence, especially at wavelengths shorter than 5500 Å, since the amount of light contributed by lower-main-sequence stars is small. On the other hand, the CN and Mg line strengths depend most strongly on atmospheric composition and to a lesser extent on the gravity along the giant branch. This latter parameter is in turn dependent on interior metal abundance, Z, because an increase in this quantity shifts the giant branch to higher gravities.

Thus, at least two parameters, mass at turnoff and metal abundance, are important in determining the integrated colors. If a mixture of populations of different ages or compositions is allowed, the problem becomes very complicated. As a first attempt, therefore, we have used the population model for the group 2 elliptical (Faber 1972) and calculated the changes in colors and line strengths that would result if only the mean metal abundance were changed. All stars in the new model have the same mass as in the original model but have a higher value of Z.

For an individual star, the continuum colors will change as a result of greater line blanketing in the atmosphere and a difference in the effective temperature caused by structural changes in the interior. These two effects are calculated separately. For the giants, Wallerstein and Helfer (1966) have calibrated $\delta(U - B)$ as a function of [Fe/H], the logarithmic iron-to-hydrogen abundance. Their relation, together with the slope of 4.0 for the blanketing vector ($\Delta(U - B)/\Delta(B - V)$) for giants given by Sandage, Becklin, and Neugebauer (1969), allows one to calculate $\Delta(U - V)$ and $\Delta(B - V)$ caused by blanketing alone as a function of [Fe/H] for the giant stars in the model. For the dwarfs near the main sequence turnoff, the blanketing vector of Wildey *et al.* (1962) and Wallerstein's (1962) calibration of $\delta(U - B)$ versus [Fe/H] were used. The light contributed by the lower-main-sequence stars to the model is negligible and can be ignored. Furthermore, we have assumed that the blanketing in $(35 - 55)$ is equal to that in $(U - V)$, while Michard's (1950) data for the Sun indicate that $\Delta(45 - 55) = 0.62\Delta(B - V)$ for small values of $\Delta(B - V)$. This relation has been assumed for giant-branch stars as well. Taken together, this body of information allows one to calculate blanketing corrections in $U - V$, $B - V$, $35 - 55$, and $45 - 55$ for all major stellar constituents in the model.

Rood's (1972) recent evolutionary tracks for a star of $0.80\ \mathfrak{M}_\odot$ indicate the effect of changes in Z on effective temperature and gravity. Considerable evidence (see below) indicates that the mean metal abundance in group 2 elliptical galaxies is roughly solar. Hence, an increase in Z over the group 2 value entails an extrapolation to compositions more metal-rich than the Sun. Unfortunately, Rood did not compute such models. We have therefore assumed that further changes in $\log T_e$ beyond those calculated by Rood can be represented by a linear extrapolation in $\log Z$ past the last computed model ($\log Z = -2.0$). This information, together with Johnson's (1966) calibration of T_e versus $U - V$ and $B - V$, yields corrections to the stellar colors $\Delta(U - V)$ and $(B - V)$ as a function of [Fe/H]. Transformation equations between the UBV system and the present 10-color system (Faber 1971) can then be used to obtain $\Delta(35 - 55)$ and $\Delta(45 - 55)$. Thus, both the blanketing and structural changes in the colors are accounted for.

Unfortunately, the change in the Mg index with [Fe/H] is not known precisely. However, McClure (1970) has investigated the effect of variations in temperature, gravity, and atmospheric abundance on the CN index $(41 - 42)$. Faber (1971, 1973*a*) has subsequently reexamined his calibration of [Fe/H] versus the CN anomaly using data on more stars. These recent results, together with Rood's models, were used to compute corrections to the model CN indices due to gravity and abundance differences

on the giant branch. The CN indices of the dwarfs near turnoff were assumed constant.

These calculations (table 12) suggest that an increase in [Fe/H] of approximately 0.30 dex represents quite closely the observed differences in colors and line strengths between elliptical galaxies in Groups 2 and 5. Two pieces of evidence indicate that the mean metal abundance in group 2 galaxies is roughly solar. First, M32 has colors typical of group 2. For the M32 models computed by Spinrad and Taylor (1971) and Faber (1972) from 36-color data, the mean abundance of the best-fitting populations is solar. Indeed, Faber (1971) has shown that one can fit the colors of M32 quite accurately by using stars of only solar composition. Second, as noted by Faber (1972), the model computed for the mean group 2 elliptical galaxy was based on stars of solar abundance and fit the observed colors well. Progressively poorer fits were obtained for groups 3 through 5, probably because the mean composition of the more luminous galaxies departs more and more widely from the solar value. In summary, within the framework of assumptions outlined above, the change in integrated colors and line strengths for the redder elliptical galaxies is consistent with an increase in [Fe/H] from the solar value to twice the solar value. This variation in [Fe/H] corresponds to a range in absolute magnitude of -17.0 to -21.3.

However, a major source of uncertainty remains. Spinrad and Taylor (1969) have argued that the SMR stars are more metal-rich than the standard curve-of-growth analyses indicate. If this is true, then the values of [Fe/H] used in calibration of color and line changes (due to blanketing effects) could be too small. However the structural corrections to the colors, arising from the change in position of the evolutionary tracks, are independent of this error. The net result is that such a scale change affects color corrections with a weight of roughly 0.50 but enters the corrections to the CN index with full weight. Consequently, the agreement between the observed and predicted continuum and line indices becomes progressively worse for large changes in the assumed abundance scale. The discrepancy is significant if one adopts the Spinrad and Taylor values for [Fe/H] for the SMR stars. However, the resultant disagreement between the continuum and line changes is not fatal because one can invoke compensatory though necessarily ad hoc changes in the turnoff mass. These will affect the continuum colors only and can be used to eliminate the discrepancy. Indeed, there is no obvious theoretical reason why two elliptical galaxies of different metal abundance should have populations with identical turnoff mass since the two populations will evolve at different rates. An additional uncertainty is the slope of the correlation between [Fe/H] and the cyanogen anomaly, which is not well determined by the data. In view of these complications, we conclude that the observed galaxy colors are consistent with the hypothesis that variations in the metal abundance alone are responsible for the differences in continuum color and line strength among the redder

TABLE 12

COMPUTED AND OBSERVED DIFFERENCES IN GALAXY COLORS AS A FUNCTION OF METAL ABUNDANCE

Δ[Fe/H]	$\Delta(35-55)$ (mag)	$\Delta(45-55)$ (mag)	$\Delta(U-V)$ (mag)	$\Delta(B-V)$ (mag)	$\Delta(41-42)$* (mag)
0.1	0.13	0.03	0.13	0.04	0.02
0.2	0.26	0.05	0.26	0.08	0.04
0.3	0.39	0.08	0.39	0.13	0.07
0.4	0.50	0.12	0.50	0.16	0.10
0.6	0.75	0.19	0.75	0.26	0.14
Observed	0.301	0.073	0.33	0.13	0.065

* On David Dunlap Observatory system.

galaxies. However, they do not prove this hypothesis. Moreover, the degree of metal enrichment necessary remains somewhat uncertain.

X. SUMMARY

The integrated colors of elliptical galaxies can be specified to a high degree of accuracy with only two independent parameters, which in turn may be utilized to determine both the intrinsic colors and the reddening between the galaxy and the observer. The intrinsic colors and line strengths are closely correlated with absolute magnitude at all luminosities. Elliptical galaxies form a sufficiently homogeneous group that they can be used to investigate galactic absorption as a function of direction. Since the strength of the absorption lines is a useful indicator of absolute magnitude, elliptical galaxies are also prime candidates for the study of anisotropy in the cosmological expansion.

Estimates of the integrated color and absorption-line changes expected from metal abundance variations alone have been calculated for an old stellar population with a main-sequence turnoff near 1 $\mathfrak{M}_\odot$. The differences in integrated photometric properties among the redder group of galaxies are consistent with an increase in [Fe/H] from the solar value to twice the solar value. No variations in turnoff mass as a function of galaxy luminosity need be invoked. However, a larger variation in metal abundance would result if the fundamental calibrations of [Fe/H] versus $\delta(U - B)$ and the cyanogen anomaly were suitably altered. In this case, a systematic variation in turnoff mass would be necessary in order to maintain consistency between the continuum and CN observations. In any case, an increase of at least a factor of 2 in mean metal abundance between the faintest and brightest galaxies in the redder group appears certain.

REFERENCES

Arp, H. C. 1962, *Ap. J.*, **135**, 311.
———. 1966, *Atlas of Peculiar Galaxies* (Pasadena: California Institute of Technology).
Baum, W. A. 1959, *Pub. A.S.P.*, **71**, 106.
Bergh, S. van den. 1960, *Ap. J.*, **131**, 558.
———. 1967, *A.J.*, **72**, 70.
———. 1970, *Nature*, **225**, 503.
Burbidge, E. M., and Burbidge, G. R. 1965, *Ap. J.*, **142**, 634.
Deeming, T. J. 1964, *M.N.R.A.S.*, **127**, 35.
Faber, S. M. 1971, unpublished Ph.D. thesis, Harvard University.
———. 1972, *Astr. and Ap.*, in press.
———. 1973*a*, *Astr. and Ap. Suppl.*, in press.
———. 1973*b*, *Ap. J. (Letters)*, in press.
Fish, R. A. 1964, *Ap. J.*, **139**, 284.
Hartwick, F. D. A. 1968, *Ap. J.*, **154**, 475.
Hayes, D. S. 1970, *Ap. J.*, **159**, 165.
Heeschen, D., and Wade, C. 1964, *A.J.*, **69**, 277.
Hodge, P. W. 1963, *A.J.*, **68**, 237.
———. 1971, *Ann. Rev. Astr. and Ap.*, **9**, 35.
Holmberg, E. 1937, *Ann. Lund Obs.*, No. 6.
———. 1958, *Medd. Lund Astr. Obs.*, Ser. II, Nr. 136.
Humason, M. L., Mayall, N. U., and Sandage, A. R. 1956, *A.J.*, **61**, 97.
Johnson, H. L. 1966, *Ann. Rev. Astr. and Ap.*, **4**, 193.
Kendall, M. G., and Stuart, A. 1966, *Advanced Theory of Statistics, Vol. 3* (London: Charles Griffin & Co.), p. 285.
King, I. R. 1971, *Pub. A.S.P.*, **83**, 377.
Lasker, B. M. 1970, *A.J.*, **75**, 21.
Martin, W., and Bingham, R. 1970, *Observatory*, **90**, 13.
McClure, R. D. 1970, *A.J.*, **71**, 41.
McClure, R. D., and Racine, R. 1969, *A.J.*, **74**, 1000.
McClure, R. D., and Bergh, S. van den. 1968*a*, *A.J.*, **73**, 1008.
———. 1968*b*, *ibid.*, **73**, 313.
Michard, R. 1950, *B.A.N.*, **11**, 227.

Mills, B., Slee, O., and Hill, E. 1958, *Australian J. Phys.*, **11**, 360.
Minkowski, R. 1961, in *Proceedings of the Fourth Berkeley Symposium on Mathematical Statistics and Probability*, ed. J. Neyman (Berkeley: University of California Press), p. 245.
Oke, J. B. 1964, *Ap. J.*, **140**, 689.
———. 1971, *ibid.*, **170**, 193.
Oke, J. B., and Sandage, A. R. 1968, *Ap. J.*, **154**, 21.
Oke, J. B., and Schild, R. E. 1970, *Ap. J.*, **161**, 1015.
Osterbrock, D. 1960, *Ap. J.*, **132**, 325.
Page, T. L. 1961, in *Proceedings of the Fourth Berkeley Symposium on Mathematical Statistics and Probability*, ed. J. Neyman (Berkeley: University of California Press), p. 277.
Rogstad, D., and Ekers, R., 1969, *Ap. J.*, **158**, 657.
Rood, H. J. 1969, *Ap. J.*, **158**, 657.
Rood, R. 1972, preprint.
Sandage, A. R. 1969, *Ap. J.*, **157**, 514.
Sandage, A. R., Becklin, E., and Neugebauer, G. 1969, *Ap. J.*, **157**, 55.
Sandage, A. R., and Wallerstein, G. 1960, *Ap. J.*, **169**, 209.
Schild, R., and Oke, J. B. 1971, *Ap. J.*, **169**, 209.
Spinrad, H., and Taylor, B. J. 1969, *Ap. J.*, **157**, 1279.
———. 1971, *Ap. J. Suppl.*, **22**, 445.
Tifft, W. G. 1969, *A.J.*, **74**, 354.
Vaucouleurs, G. de. 1961, *Ap. J. Suppl.*, **5**, 233.
Vaucouleurs, G. de, and Malik, G. 1969, *M.N.R.A.S.*, **142**, 429.
Vaucouleurs, G. de, and Vaucouleurs, A. de. 1964, *Reference Catalogue of Bright Galaxies* (Austin: University of Texas Press).
Wallerstein, G. 1962, *Ap. J. Suppl.*, **6**, 407.
Wallerstein, G., and Helfer, H. L. 1966, *A.J.*, **71**, 350.
Webb, C. J. 1964, *A.J.*, **69**, 442.
Whitford, A. E. 1958, *A.J.*, **63**, 201.
———. 1971, *Ap. J.*, **169**, 215.
Wildey, R. L., Burbidge, E. M., Sandage, A. R., and Burbidge, G. R. 1962, *Ap. J.*, **135**, 94.
Wood, D. B. 1966, *Ap. J.*, **145**, 36.
———. 1969, *A.J.*, **74**, 177.